Pakistan Journal of Engineering Technology and Science (PJETS)
Volume 13. Issue.2, PP. 69-88, December 2025
https://doi.org/10.22555/pjets.v13i2.1457
E-ISSN 2224-2333
P-ISSN 2222-9930

An Islanding Detection and Control Algorithm based on CVFR for Voltage Source Converter in CIGRE LV Network

Sheikh Junaid Yawar[1], Muhammad Raza[2*], Aurangzeb Rashid Masud[3], Amna Aslam[4], Muhammad Ovais Akhter[5], Faisal Siddiqui[6]
[1]Electrical Engineering Department, Sir Syed University of Engineering and Technology, Karachi, Pakistan
[2,3,4,5]Bahria School of Engineering and Applied Sciences, Bahria University, Karachi Campus, Pakistan
[6]Sustainable Energies Enterprise, Karachi, Pakistan
[*]Corresponding Author: Muhammad Raza, mraza.bukc@bahria.edu.pk

Abstract:

Distributed Generators (DGs) are widely used as Distributed Energy Resources (DERs) and have become an integral part of modern distribution systems. Although these DGs improve the voltage profile and reduce power losses, they have introduced challenges such as islanding and safety issues. This article proposes a control technique for the islanding detection and control of Voltage Source Converters (VSCs) based on Combined Voltage and Frequency Relays (CVFR). The CVFR control structure is designed to detect the presence of islanding with minimal detection time and can change the mode of operation of the VSC to provide a stable voltage supply to the connected load. The effectiveness of the proposed scheme has been studied on the CIGRE LV Test Network with six sets of DGs using a passive detection technique. The performance of the control scheme has been tested in a number of scenarios, with simulation and comparison made with other detection techniques to validate the model. The system has been modeled and simulated using the software, Matlab/Simulink.

Keywords: *Frequency control, Island detection, Microgrid, Voltage control, VSC.*

I. INTRODUCTION

The rapid development of renewable energy sources (RES) in modern power distribution networks has brought a significant shift towards distributed generation (DG). This change is primarily observed under low-voltage (LV) network environments. Renewable Energy Systems (RES) have also changed the traditional centralized power systems substantially to decentralized systems and have introduced Microgrids (MGs) that have presented novel configurations of the energy systems. This has also opened new avenues for researchers to examine the impacts of renewable energy systems and their accessories on the traditional power systems [1]. Renewable energy systems utilize integrated Distributed Generators (DGs) area of the grid that has gained popularity because of the usage of green RES such as wind, solar, and fuel cells. The long use of conventional Power Generation Systems that utilize fossil fuels & coal has caused adverse environmental impacts, including the greenhouse effect. In contrast, DGs integration is serving to alleviate these issues via sustainability and reducing carbon emissions [2]. Figure 1 represents a standard microgrid system.

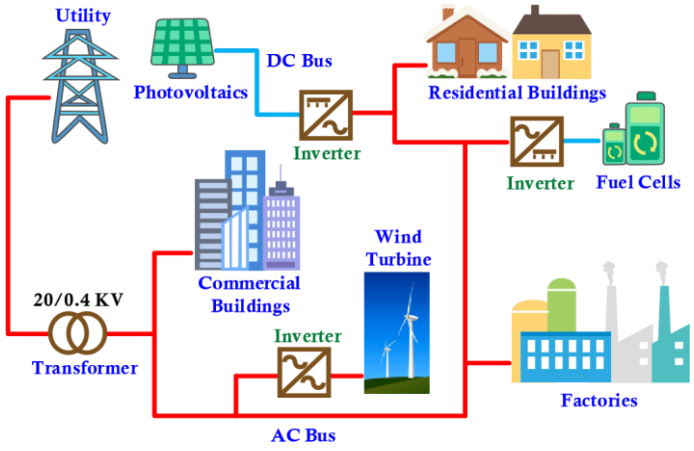

Figure 1: Modern Microgrid having inverters

The Microgrid (MG) system combines both AC and DC buses to integrate the renewable sources. Voltage Source Converters (VSCs) convert DC to AC. These converters supply the AC power to the load and identify islanding to ensure the proper functioning of the system. Usually, Microgrids have DC loads, including electric vehicles, industrial DC appliances, and residential and commercial building appliances.

The VSCs are connected to the load and Distributed Generators (DGs). Nonetheless, DGs' usage has brought several problems to the power system, and islanding is one of the primary concerns [3]. Islanding is a situation that occurs when the circuit breaker is opened at the utility end, but the Distributed Generator (wind, fuel cell, or solar) keeps supplying power to the load. It offers continuous power to the load even when it is taken off from the utility grid. Islanding poses a hazardous situation for the utility workers poses a risk because they may not be aware of whether the circuit is energized due to the auto-closure of the devices. Furthermore, disconnection from the utility will deteriorate the system's power quality. This is useful for starting various power plants to restore the system [4]. As Distributed Generators (DGs) increase in electrical distribution networks, they introduce challenges to the infrastructure of modern grid systems, such as power coordination problems, voltage regulation issues, and Total Harmonic Distortion (THD) [5]. To detect the islanding condition, there must be an accurate and efficient mechanism that responds to changes in system parameters to alter the mode of operation of the Distributed Generator (DG) or prevent unintentional islanding [6]. Figure 2 shows the proposed islanding detection scheme under consideration.

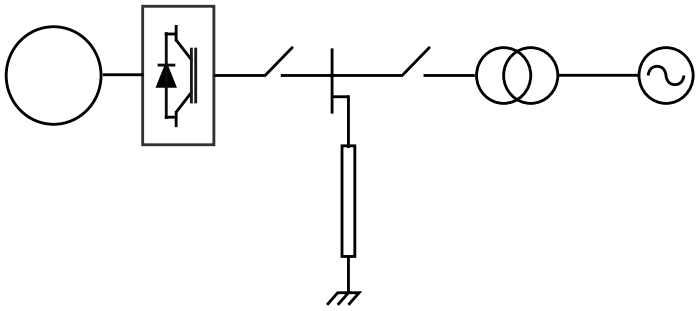

Figure 2: Proposed islanding detection scheme

There are two circuit breakers: CB1 at the DG end and CB2 at the utility end. During normal conditions, both circuit breakers are in the closed position. When circuit breaker CB2 opens due to a fault, there is a significant change in the system's Total Harmonic Distortion (THD), voltage, and frequency. These voltage and frequency changes are sensed

by the Voltage Source Converter (VSC) controller. When the variations exceed the defined thresholds, the VSC switches its mode of operation from grid-following mode.

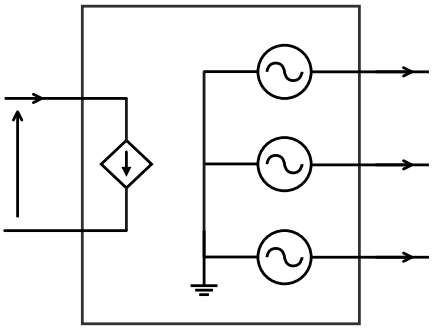

Figure 3: Average Model of Converter

Here, the average model of the Voltage Source Converter (VSC) is used for the analysis as it is more efficient and faster compared to the switching model [7]. Analysis is performed on a low-voltage three-phase system. Figure 3 depicts the average model scheme applied with the design model having the VSC. The Voltage Source Converter (VSC) is first used in grid-following mode synchronized with the frequency of the utility grid. When islanding conditions occur due to any fault, the VSC separates itself from the utility grid and smoothly switches to grid-forming mode to ensure a constant power flow to the load it is applied to.

A. Motivation:

Despite the significant progress made so far in islanding detection techniques, most of the passive methods developed to date, e.g., simple over/under-voltage and over/under-frequency relays-suffer from large Non-Detection Zones (NDZ), slow response times, or failure to ensure seamless power continuity to critical loads in the case of unintentional islanding. Active and hybrid methods, although reducing NDZ, degrade the power quality due to continuous or periodic disturbance injection and are less effective when multiple inverter-based DGs operate in parallel.

Moreover, hardly any of the research work has focused on immediate post-detection action; most stop at the issuance of a trip command, leaving the local load unpowered. In the modern low-voltage microgrids with high renewable penetration, disconnecting the load is no longer acceptable, especially for residential and small commercial consumers expecting an uninterrupted supply.

This work is motivated by the need for a fast, reliable, and completely passive islanding detection method that is capable of not only detecting the loss of mains with minimum delay but also automatically reconfiguring the VSC from grid-following to grid-forming mode so that stable voltage and frequency are maintained for the local load without any active signal injection or external communication.

B. Contribution:

The novel contributions of this paper are summarized explicitly as follows:

1. Design and validate a CVFR-based passive islanding detection scheme that regularly produces detection times less than 200ms on the CIGRE European LV benchmark network, while conventional OUV/OUF and ROCOF relays give higher detection times under identical conditions.
2. Seamless and automatic mode-transition control of a single VSC from grid-following to grid-forming operation instantly when islanding is detected based on only local measurements and using standard control equations given by (6) – (7), for delivering uninterrupted, high-quality power to the local load.
3. Demonstration that a purely passive method can concurrently offer small NDZ, zero power quality degradation, and ride through capability in inverter-dominated low voltage microgrids, something that has never been done before in literature.

4. Extensive performance comparison with state-of-the-art passive relays, namely, ROCOF and classical OUV, demonstrating faster and more reliable detection without the need for either communication or disturbance injection.

These contributions bridge the gap between traditional anti-islanding protection and modern microgrid resilience requirements to collectively enable true "self-healing" capability at the low-voltage customer level.

To present the details of the study, this paper is organized as follows: Section I is the introduction that describes the background and problem statement of the study. Section II gives a comprehensive literature review of the study performed. The methodology followed for the study is given in Section III. Experimental results and discussion on the findings are given in Section IV at length. Section V gives the conclusion of the study.

II. LITERATURE REVIEW

Microgrids have been introduced as an effective option in the assimilation of renewable power sources into contemporary power frameworks and while preserving flexibility, dependability, and sustainability of energy. However, Islanding detection is still one of the most important operational challenges of microgrids, which is the ability to properly anticipate the unintentional and unprecedented disconnection to the main grid to avoid damage to equipment and safety risks. Extensive studies have been carried out to improve islanding detection methods, better control schemes, and seamless transitions between grid-connected and island modes.

Kazmierkowski, Krishnan, and Blaabjerg provided the key insight into the principles of converter control in power electronics that remain the basis of the modern inverter design strategy [8]. From the VSC control systems perspective, Song, Lynch, and Dinavahi validated the nonlinear control system of voltage source converters (VSCs), which gave experimental evidence of better performance under dynamic conditions [7]. Ghaderi and Kalantar investigated the effects of the system parameters on passive detection schemes and observed that an inverter-based distributed generation (DG) system has peculiar issues due to the reduced fault current contribution [9]. Hoke and Maksimovic made contributions to the active power control in photovoltaic systems by demonstrating the importance of the coordinated control of the inverter to the energy balance and islanding avoidance [10]. Banu et al. made a comparative analysis of anti-islanding schemes in grid-tied photovoltaic systems and formulated criteria to judge the robustness of the technique and standard adherents [11]. Mohan et al. addressed the issue of microgrid energy management by integrating uncertainties in renewable power generation and load demand using probabilistic methods to enhance the decision-making process in microgrid functioning [12]. Ortiz et al. simulated and modeled hybrid AC/DC microgrids in grid-connected mode, which provides information about interoperability and control design [3]. Aghazedeh et al. analyzed the operation of dual two-level voltage-source inverter behavior under varying grid impedance and PLL dynamics, which provided an informative contribution to enhance robust grid integration [13]. Waghare and Bhasme also explored the issue of islanding detection in distributed generation systems during fault events when the loads that require protection are critical and non-critical [14]. Sayed and Massoud established a MATLAB/Simulink-based average-value model of a multi-terminal HVDC network and used it to study DC grid integration and fault behavior [15]. Elshrief et al. designed a quick and exact islanding detection method in PV-based microgrids that focuses on real-time implementability and minimal computational load [16]. Kumar, Kumar, and Tyagi investigated the islanding detection in reconfigurable micro grids using renewable energy sources (RES), where adaptive mechanisms are suggested to enhance the speed and accuracy of detection [4]. In the same manner, Hasan and Saleh proposed a new transient energy-based passive islanding detection method, which has a better sensitivity in a wide range of operating conditions [17]. The survey of islanding detection techniques of microgrids carried out by Cebollero et al. compared both the active and passive approaches to identify islanding detection and its efficiency against the international grid codes [1]. Their paper focused on the significance of reducing Non-Detection Zones (NDZ) in the quest to achieve robust and reliable performance of the islanding detection. In a complementary study, Panchal et al. carried out a comparative study of the islanding detection methods of microgrids coupled with solar PV systems and pointed out

the efficiency of the hybrid strategies that use both passive and active strategies [6]. Fault and islanding detection have been increasingly subjected to advanced computational and signal processing techniques. A hybrid optimized kernel extreme learning machine (HOKELM) based on Fast Fourier Discrete Orthonormal Stockwell Transform of fault detection in DG-integrated microgrids was proposed by Sarangi, Sahu, and Rout [2]. Their method showed high precision in the detection of disturbances and enhancement of reliability. Microgrid stability is still maintained by control and protection technologies. Nanda, Panda, and Panigrahi reviewed different schemes of control to solve islanding problems, in particular, the distributed generation control and voltage/frequency control [5].

Chen et al. progressed the research by presenting a generalized multivariate grid-forming control design of power converters, which demonstrates the significance of converter control by sustaining the grid stability under varying conditions [18]. Another key issue in microgrids is protection coordination. Luo, Nutkani, and Meegahapola proposed an adaptive protection scheme that combines passive islanding detection techniques of AC micro grids so that false tripping is minimized without sensitivity loss [19]. In the same line, Zhou et al. examined the small-signal stability of heterogeneous grid-following converter systems, and they found that the stability is intrinsically dependent on grid strength and converter interactions [20]. All these studies support the significance of the adaptive and smart protection systems in the future architecture of microgrids. Neither Cebollero et al. [1] nor Nanda et al. underrated the importance of matching technical developments to changes in the grid codes to provide interoperability and safety [5]. Zheng et al. have suggested a method of identifying islanding in microgrids in which synchronized small-AC-signal injection is used to identify islanding [21]. Their approach makes use of a controlled AC signal injection and system response analysis to achieve high detection accuracy and low non-detection regions. This solution is especially suitable for those microgrids that have inverters as the dominant feature, which is a reliable solution to the new grid setup. Ramos et al. investigated the effects of output voltage control on islanding detection of PV generation systems [22]. Their results show that the strategies to regulate voltage largely influence the operation of detection algorithms when it comes to high-penetration PV situations. The research highlights the need for adaptive control mechanisms to improve the reliability of detection in different operating conditions. Another contribution was made by Chaudhary et al., who came up with a fast passive anti-islanding approach to AC microgrids using a cubature Kalman filtering algorithm [23]. This method makes use of developed signal processing to get quick and accurate identification of islanding. The authors proved its usefulness in AC microgrids that have variable loads, and it is much faster and stronger than the traditional passive approaches. Active detection techniques have also been developed, especially for grid-forming inverters.

While the aforementioned studies have advanced islanding detection through various passive, active, and hybrid techniques such as signal injection [21], voltage regulation impacts [22], and Kalman filtering for rapid identification [23] they often suffer from limitations including larger non-detection zones (NDZ), higher computational complexity, susceptibility to noise in dynamic conditions, and inadequate focus on seamless mode transitions for Voltage Source Converters (VSCs) in low voltage networks. For instance, methods like ROCOF or OUV relays [11, 14] exhibit slower response times during frequency or voltage deviations, potentially leading to instability or delayed power restoration. In contrast, this work proposes a novel Combined Voltage and Frequency Relay (CVFR) based technique that integrates passive detection with relay logic to achieve minimal detection times (e.g., under 200ms in simulations) while enabling automatic switching from grid-following to grid-forming modes, ensuring stable voltage supply to loads without injecting perturbations. By leveraging an average VSC model in the CIGRE LV Test Network and validating against IEEE 1547 standards, this approach addresses these gaps by reducing NDZ, enhancing robustness under varied load conditions, and providing faster, more reliable performance compared to conventional relays, as demonstrated through comparative simulations.

III. METHODOLOGY FOR ISLANDING DETECTION AND DETECTION OF VSC

A. Islanding Detection Techniques:

Islanding detection methods are broadly categorized into local and remote detection methods. The local detection method is further divided into active, passive, and hybrid methods. In the active method, current is applied to the

system, and changes are monitored to identify the islanding. The passive method is based on the measurement of the Point of Common Coupling (PCC) to determine frequency, voltage, and harmonic variations to detect islanding. Whereas the hybrid approach incorporates the features of both active and passive methods. Among these, the passive technique is preferred, as it has the merits of fast detection and the absence of injected currents. Moreover, its efficiency doesn't decline when several Distributed Generators (DGs) are incorporated into the system [17]. Considering these advantages, this study recommends the implementation of the passive technique of detection.

This choice is justified by the theoretical assumption that islanding events cause detectable deviations in voltage and frequency due to imbalances in active and reactive power between the DG and the load, as governed by the generator swing equation for frequency and AVR droop for voltage. Passive methods rely on local measurements at the PCC without injecting disturbances, minimizing impact on power quality and ensuring compatibility with multiple DGs, unlike active methods, which may introduce harmonics or increase NDZ in noisy environments.

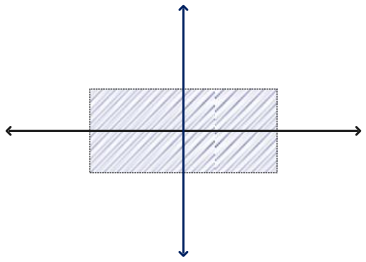

Figure 4: Variation of voltage and frequency

The introduction and removal of the loads on a generator interfere with active and reactive power flow in the system and cause shifts in the frequency and voltage parameters. The larger the difference in the magnitude of power, the larger the deviations in the frequency and the voltage [9]. An active power is applied by the utility that is stronger than the load demand leads to over-frequency (OF), and an active power that is less than the load demand leads to under-frequency (UF). Equally, under-voltage (UV) and over-voltage (OV) are caused by a deficit and surplus of reactive power, respectively, by the utility in the system [10], as shown in Figure 4. The active power balance is controlled by the mechanical properties of a synchronous generator, which is dependent on the rotor angle and the governor control, to control the frequency of the generator, as explained by the generator swing equation. The gain of the governor droop (P) is directly proportional to the governor droop gain, resulting in over-frequency as the active power supply of the generator is increased. Similarly, the Automatic Voltage Regulator (AVR) droop gain is directly proportional to the reactive power (Q), and the droop gain controls the output voltage [8].

$$\Delta P = P_{load} - P_{grid} \quad (1)$$

$$\Delta Q = Q_{load} - Q_{grid} \quad (2)$$

The active power change is directly proportional to the frequency change, and the reactive power change is directly proportional to the voltage change. This proportionality assumes a linear response in the system's mechanical and electrical dynamics under small perturbations, valid for typical microgrid operations where power mismatches exceed relay sensitivities. Islanding is determined by over-/under-voltage relays and/or under-frequency relays [19]. The relays have to be rapid and effective to detect the islanding condition and change the operating mode of the Distributed Generator (DG). This paper will therefore consider a scheme of detection of islanding by the use of relays, which can identify fast islanding, and the performance is similar to other relay-based schemes. The efficiency of the suggested method is proven by the tests in different load conditions.

B. CIGRGE LV Network:

The passive method of detecting islanding in the CIGRE Low-Voltage (LV) Network at 230 Vrms phase to phase is used. The CIGRE LV network is selected as the test system because it serves as a standardized benchmark for

European-style low-voltage distribution networks, incorporating realistic topologies, loads, and DG integrations, enabling comparable and reproducible results across studies on islanding and microgrid control. Simulation of the islanding detection scheme was done in MATLAB/ Simulink R2020a using frequency and voltage disturbance measurements at the Point of Common Coupling (PCC). The parameter limits of islanding detection are outlined in IEEE Standard 1547, which is the threshold to be compared, and the details are given in Table 1. The specifications of Distributed Generation Systems are given by the Institute of Electrical and Electronics Engineers (IEEE); the IEEE standard 1547 sets the requirements of the interconnection between the distributed generators (DGs) and the grid [16].

Table 1: Details of IEEE Thresholds

Standard Thresholds	Details
88 % ≤ V ≤ 110%	The voltage at PCC below 202.4Vrms per phase will be considered as Under Voltage (UV). The Voltage above 253Vrms per phase will be considered as Over Voltage (OV).
49.5Hz ≤ f ≤ 50.5Hz	The frequency at PCC below 49.5 Hz will be considered as Under Frequency (UF). The Frequency above 50.5 Hz will be considered as Over Frequency.
Time 2s	This is the maximum time in which Islanding must be detected.
THD ≤ 5 %	Total Harmonic Distortion should be less than 5 % in the system.

C. Studied System:

The developed model of Voltage Source Converter (VSC) is applied in the CIGRE Low-Voltage (LV) Network as shown in Figure 5, i.e., the inverter No. 3 with an 18kVA rating is used to provide an 8.8kVA single household load. The major distributed energy source is a 15kW photovoltaic (PV) system. The islanding detecting mechanism uses frequency and voltage relays that use a passive detecting method to detect islanding by observing variations at the Point of Common Coupling (PCC). The control logic incorporated in the VSC control system allows for a smooth switch between the grid-following and grid-forming operation modes of the VSC to maintain stable power delivery in case of an islanding event. The system will be connected to the grid at a medium voltage of 20kV, and it will be interfaced by a transformer with a 20kV to 0.4kV primary to secondary turns ratio as stated in the CIGRE LV Network. The VSC links to the low-voltage side of the transformer at 400 V line-to-line, and the power is supplied to the consumer end.

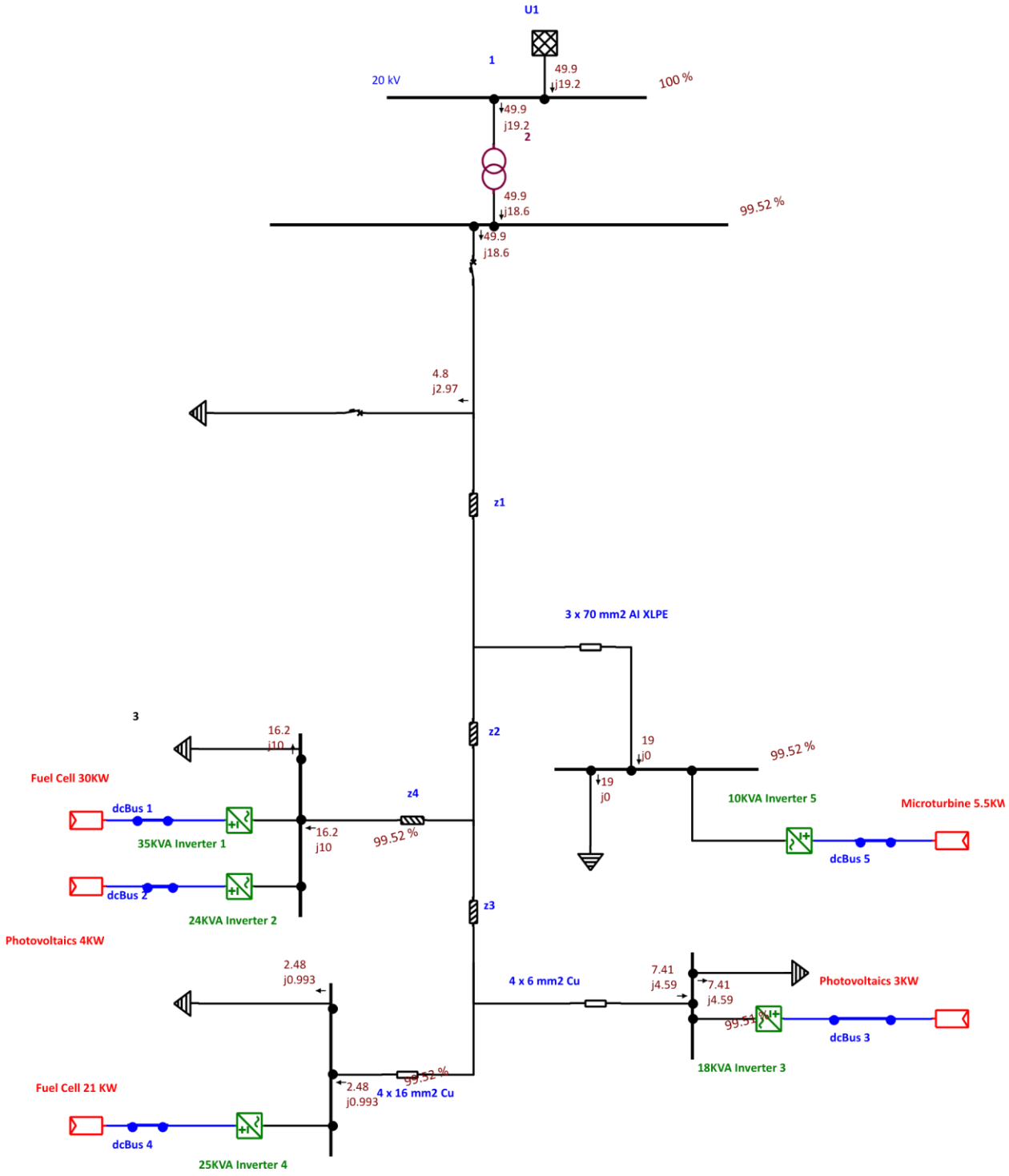

Figure 5: CIGRE Low Voltage Network for System Analysis

D. VSC Modeling:

The ideal AC voltage source is the grid-forming converter, which needs a reference generator to program the frequency (ω) and voltage (E) with the result being an AC power supply at a desired frequency ω, as shown in Figure 6(a). The use of the average model for VSC analysis assumes that the switching frequency is sufficiently high relative to the

fundamental frequency, allowing the neglect of high-frequency ripples and focusing on average behavior for faster simulation times and control design, which is particularly efficient for studying transient responses in microgrids compared to detailed switching models.

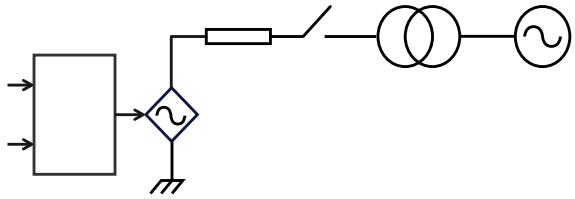

Figure 6(a): Representation of Grid Forming Converter

These converters, which are usually connected to renewable energy sources, e.g., solar photovoltaic systems, produce a sinusoidal AC signal. Voltage and current control loops are controlled by the direct-quadrature (dq) reference frame, which controls the external and internal control loops, respectively [18].

On the other hand, a perfect current source is an icon of the grid-following converter, which conveys energy to the load or the grid. Such converters generate an AC waveform of voltage that is completely synchronized to the grid to allow the export of energy, as shown in Figure 6(b). To make certain that a Phase-Locked Loop (PLL) is operating properly, the frequency ω is monitored at the Point of Common Coupling (PCC). These converters have active and reactive power controllers that control the amount of power supplied to the load in accordance with the requirements.

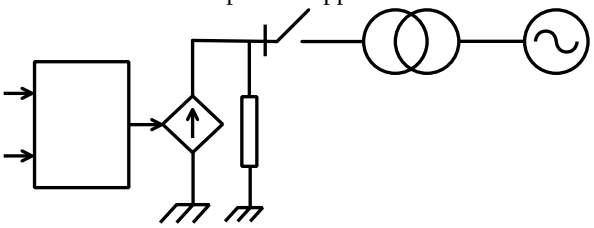

Figure 6(b): Representation of Grid Following Converter

The active and reactive power that the converters are required to provide are P and Q, respectively. These converters have high input impedance, which allows them to be connected in parallel with other converters, but they cannot be used in an islanding mode [20]

Initially, the Voltage Source Converter (VSC) operates in grid-following mode, synchronized with the grid frequency ω. The three-phase balanced voltages of the VSC are represented by mathematical equations, as detailed below.

$$v_a(t) = V_m \sin(wt + \emptyset) \quad (3)$$

$$v_b(t) = V_m \sin(wt - 2\pi/3 + \emptyset) \quad (4)$$

$$v_c(t) = V_m \sin(wt - 4\pi/3 + \emptyset) \quad (5)$$

The three-phase voltages generated by the Voltage Source Converter (VSC) are compared against the threshold limits specified in IEEE Standard 1547, as represented by equations (6–7). These limits ensure that the voltage and frequency measured at the Point of Common Coupling (PCC) remain within acceptable bounds; otherwise, an islanding condition is detected.

$$\left(\frac{V}{V_{max}}\right)^2 - 1 \leq \frac{\Delta F}{F} \leq \left(\frac{V}{V_{min}}\right)^2 - 1 \quad (6)$$

$$1 - \left(\frac{f}{\quad}\right)^2 \leq \frac{\Delta V}{\quad} \leq 1 - \left(\frac{f}{\quad}\right)^2 \quad (7)$$

f_{min} V f_{max}

Park's transform converts the three-phase voltages Va, Vb, and Vc into a time variant signal in a dq_O rotating coordinate frame [15]. This transformation assumes a balanced three-phase system, enabling decoupled control of active (d-axis) and reactive (q-axis) power, which simplifies PI controller design and improves dynamic performance under nominal conditions.

$$V_{d,i} \quad \sin\theta \quad \sin\left(\frac{2\pi}{3}(\theta -\right) \quad \sin\left(\frac{4\pi}{3}(\theta -\right) \quad V_a$$

$$[VV_{q0,i}] = \begin{matrix} cos\theta & \cos(\theta -\frac{2\pi}{3}) & \cos(\theta -\frac{4\pi}{3}) \\ [1/2 & 1/2 & 1/2 \end{matrix} \quad [VV_{cb}] \quad] \qquad (8)$$

The relationship between the VSC and utility in the *dq* frame [13] is expressed by (9-18) using Kirchhoff's law.

$$u_{dq} = [u_d, u_q]^T \qquad (9)$$

$$V_{t,dqi} = R_{T,i}\, i_{dq,i} + L_{T,i}\frac{di_{dq,i}}{dt} \pm wL_{T,i}\, i_{dq,i} + V_{dq,i} \qquad (10)$$

For the control signal *U*

$$U_{t,dqi} = R_{T,i}\, i_{dq,i} + L_{T,i}\frac{di_{dq,i}}{dt} \qquad (11)$$

$$V_{t,dqi} = U_{t,dqi} \pm wL_{T,i}\, i_{dq,i} + V_{dq,i} \qquad (12)$$

It can be presented by the following control signals

$$U_{t,dqi} = (K_{dq,Pi}\, i_{dq,i} + \frac{K_{dq,Ii}}{s})(i_{dq,i}* - i_{dq,i}) \qquad (13)$$

Where $K_{dq,Pi}$ and $K_{dq,Ii}$ are the gains for the PI (Proportional-Integral) Controller

$$V_{t,dqi}* = (K_{dq,Pi} + \frac{K_{dq,Ii}}{s})(i_{dq,i}* - i_{dq,i}) \pm wL_{T,i}\, i_{dq,i} + V_{dq,i} \qquad (14)$$

The instantaneous active and reactive power injected are given as:

$$P_{gi} = V_{d,i}\, i_{d,i} \qquad (15)$$

$$Q_{gi} = -V_{d,i}\, i_{q,i} \quad (16).$$ The corresponding active and reactive currents are obtained by

$$i_{d,i}* = (K_{d,Pi} + \frac{K_{d,Ii}}{s})\left[\Delta P_{g,i}\frac{1}{K_i} + (\Delta V_{gi})\right] \qquad (17)$$

$$i_{q,i}* = (K_{q,Pi} + \frac{K_{q,Ii}}{s})(\Delta Q_{g,i}) \qquad (18)$$

E. System Parameters

A three-phase, two-level voltage source converter simulation model is developed as seen in Figure 7. The DC link voltage is chosen to be approximately 1.5-2 times the peak line-to-line AC voltage to provide adequate modulation index margin, prevent overmodulation, and ensure stable operation during transients, aligning with common practices in LV VSC designs for 400V grids. Other parameters, such as filter inductances and capacitances, are tuned based on resonance frequency considerations (set half the switching frequency) to dampen oscillations and meet THD limits per grid codes.

Modeling is done using the "Universal Bridge" block from the Simscape SimPowerSystems package in Simulink. These blocks give a clear view of the VSC subsystem and help analyze its performance in simulation. The transformer data was taken from Schneider Electric's oil-type transformer sheets to keep the model realistic [21]. It has a 400kVA rating with a 20-kV primary and a 400 V secondary, following IEC 60076 standards. In Simulink, a three-phase programmable voltage source rated at 1 MVA represents the utility grid. This configuration permits testing of conditions such as over-voltage, under-voltage, over-frequency, and under-frequency.

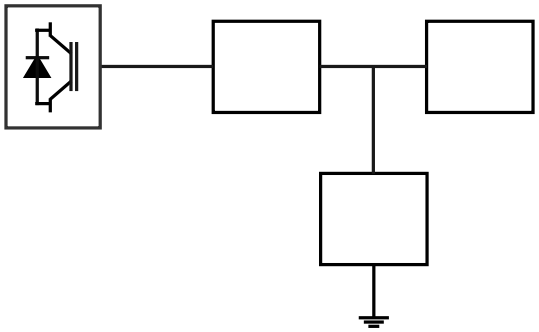

Figure 7: VSC Subsystem

The block shown in Figure 8 incorporates control circuitry for the VSC mode transition and integrated frequency and voltage relays for islanding detection.

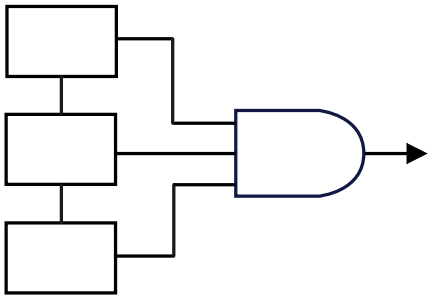

Figure 8: Detection and Control Subsystem

The frequency at the PCC is measured by a PLL Simulink block, and the voltages and currents are tracked by a three-phase measurement block. Table 2 lists all the network and VSC parameters that were used in the Simulink model.

Table 2: Simulink Modeling Parameters

Variable	Value	Unit
Grid Voltages (Line to Line)	20	KV
Transformer Apparent Power	400	KVA
Transformer Ratio	20/0.4	KV
Transformer Resistance	0.12	Ω
Transformer Inductance	2	H
No load losses	445.1	W
Load-losses	3575	W
Phase Voltage (Line to Ground)	230	VAC
Line Voltage (Line to Line)	400	VAC
Load Active Power	7480	W
Load Reactive Power	1320	VAR
Rated DC Voltage of DG	715.59	VDC
Capacitance of AC Filter	50	µF
Resistance of AC Filter	0.1	Ω
Inductance of AC Filter	3.5	mH
Reactor Resistance	0.05	Ω
Reactance Inductance	0.35	mH
Frequency	50	Hz
Angular Frequency	314.16	rad/sec
PI Current Controller Gains	157.23+5.503/s	

IV. RESULTS AND DISCUSSION

The simulation results obtained using MATLAB/Simulink are discussed in this section. The system's performance under different operating conditions is evaluated. In the simulation setup, a grid connected to a 20kV bus through a 400kVA transformer, with a 20kV primary voltage and a 400V secondary voltage line-to-line voltage. A converter, rated at 18kVA, is connected on the low-voltage side and supplies a load at the PCC. The load requires 1320VAR of reactive power and 7480W of active power. The system is first analyzed under normal operating conditions before the introduction of any fault. During this pre-fault period, the load receives a balanced three-phase supply from the converter with stable voltage and current waveforms observed at the PCC, as shown in Figure 9(a). All voltage waveforms are sinusoidal and symmetrical by nature, each having a peak amplitude value of about 325V, which corresponds to an RMS value of 230V per phase.

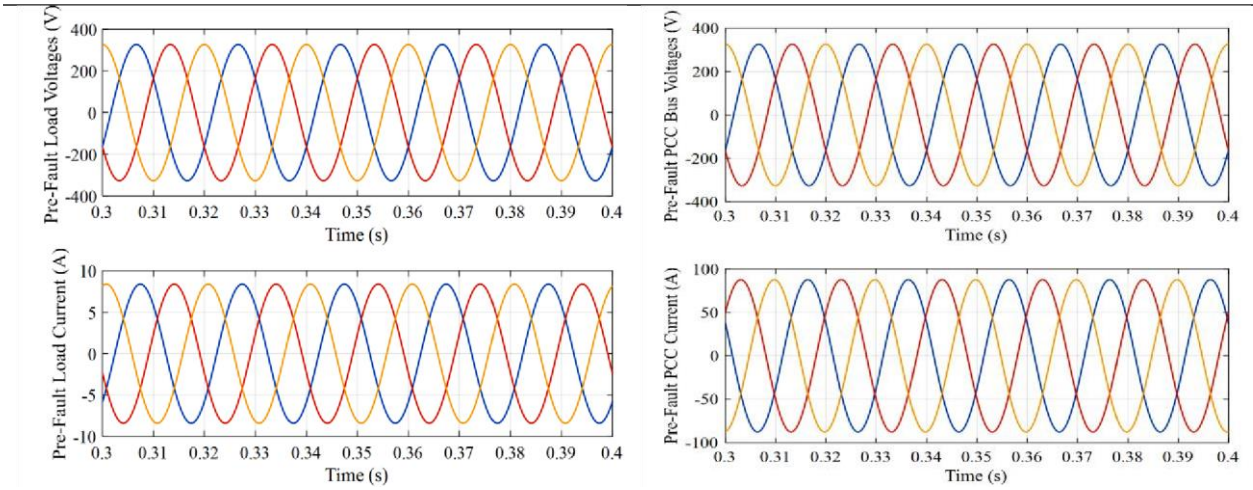

(a) **(b)**

Figure 9: Voltage and Current at (a) Pre-Fault Load (b) Pre-Fault PCC Bus

The load currents are also balanced with peak values near 10.6A with RMS approximately 7.5A. The waveforms retain a sinusoidal shape with low harmonic distortion and exhibit a consistent 50 Hz frequency corresponding to a period of approximately 20ms. The converter's output at the PCC during loaded conditions is shown in Figure 9(b). The phase voltages peak around 325V, and load currents reach around 90 A. These statistics express the estimated output delivery of 7480W active power and 1320VAR reactive power.

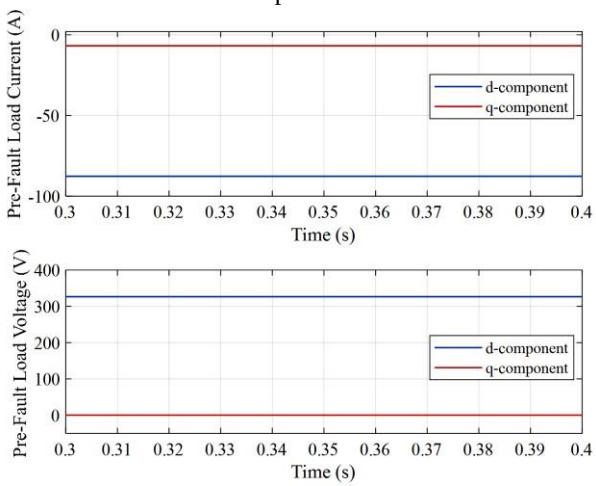

Figure 10: Pre-Fault Voltage and Current in the dq Reference Frame

The waveforms of the three-phase voltage and current remain in phase and aligned. There is no discernible imbalance between the stages. This shows that the converter controls both active and reactive power flows while maintaining synchronization. The time-domain signals are analyzed in the synchronous rotating reference frame (dq frame) to decouple and control active and reactive power independently. The I_d and V_d components from the PI controller are presented in Figure 10. The pre-fault dq frame analysis shows that the d-axis voltage stabilizes at approximately 325V. The q-axis voltage remains close to zero. This indicates that the voltage vector is aligned with the d-axis in the rotating reference frame. As a result, the control system can regulate voltage using only the d-axis component. The d-axis current reaches around 75A, showing that the system is delivering active power to the load. The q-axis current shows relatively small reactive power flow. The voltage behavior at the PCC and converter terminals during the shift from grid-following to grid-forming operation under an undervoltage islanding condition is shown in Figure 11(a). According to IEEE 1574 standards, islanding occurs when the RMS voltage per phase drops below 202.4V. In this

simulation, the PCC voltage falls below this threshold at 0.517s, marking the start of the under-voltage condition. During the grid-following period, the converter operates by tracking the grid reference signals. But as the grid voltage weakens, a noticeable distortion and oscillations appear in the output waveform. Islanding is detected at 0.692s, which then triggers a shift in the converter's control strategy.

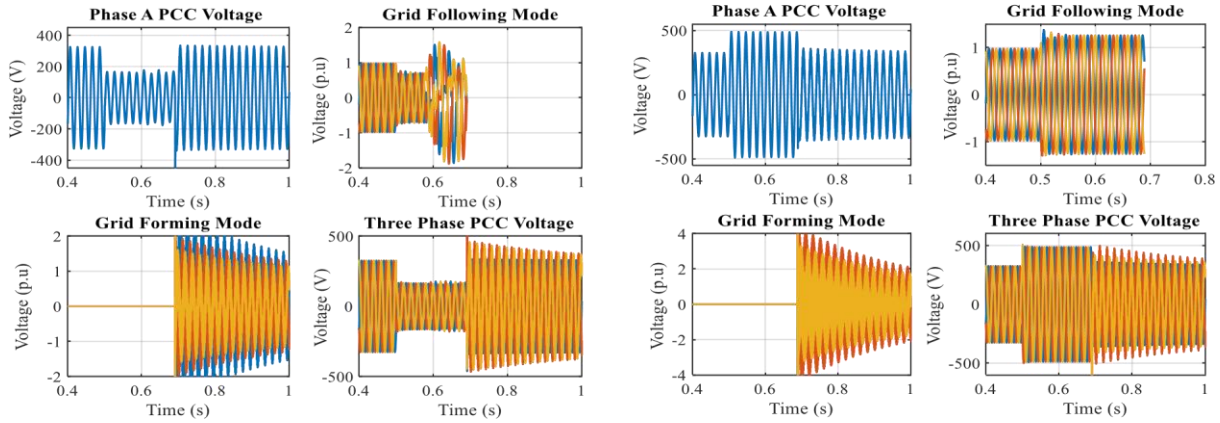

(a) **(b)**

Figure 11: Operation of Converter during (a) Under Voltage Condition (b) Over Voltage Condition

The converter switches into grid-forming mode at 0.696s, that is 178.516ms after the voltage sag is noticed by the system. Grid-forming means controlling the PCC voltage and bringing waveform stability back while maintaining balanced three-phase voltages.

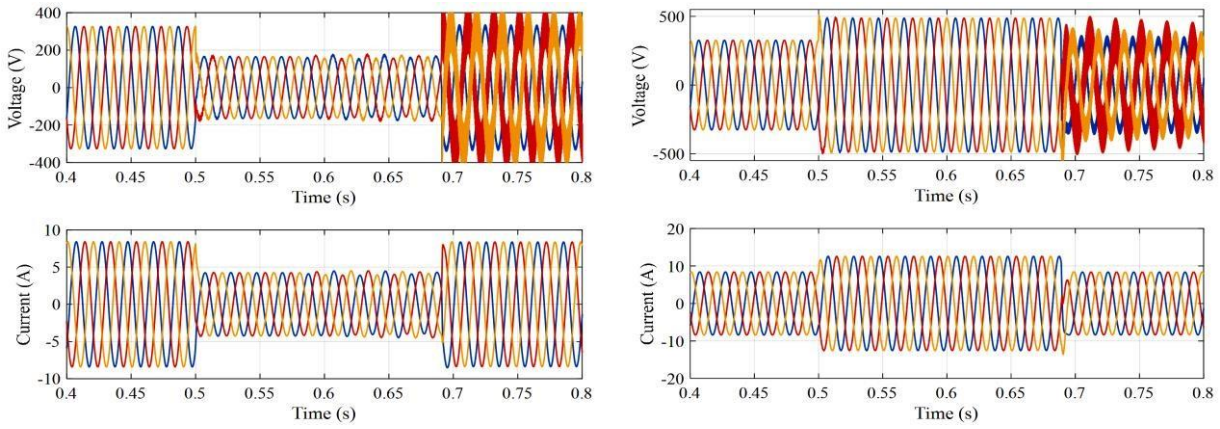

(a) **(b)**

Figure 12: Converter Load Current and Voltage during (a) Under Voltage Condition (b) Over Voltage Condition

The overvoltage condition for islanding detection will be when the RMS voltage per phase crosses 252V, as recommended by IEEE 1547 standards. In this simulation, per-phase voltage at PCC exceeds 252Vrms at 0.508s; hence islanding will be detected later at 0.689s., After this detection, the VSC changes its operation from grid-following to grid-forming at 0.692 seconds, which translates to 181.818ms after the overvoltage event has taken place. The PCC voltage and converter output in both operating modes are depicted in Figure 11(b). The waveforms of voltage and current at the load end in an undervoltage situation are presented in Figure 12(a).

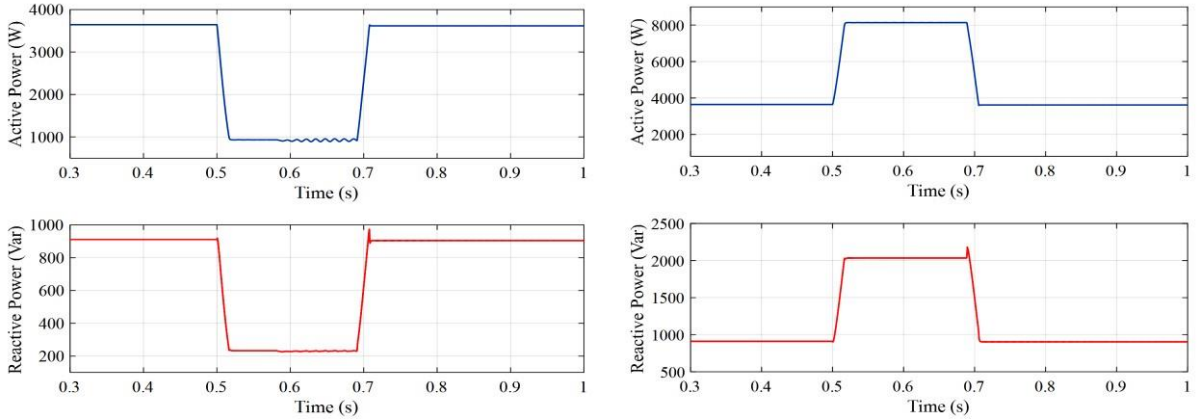

(a) **(b)**

Figure 13: Active and Reactive Power at Load End (a) Under Voltage Condition (b) Over Voltage Condition

A three-phase output stable at 0.705s, which is about 189.017ms after detection of undervoltage. Once the system transitions to the grid-forming mode, the converter maintains a steady and balanced supply to the load. Both voltage and current waveforms show the restoration of normal operation and the system's capability to withstand stable output despite the grid disturbance. The profiles for current and voltage at the load end during disturbance and subsequent steady-state operation are shown in Figure 12(b). A top left graph reflects a significant increase in voltage amplitude alongside current oscillations during this period of disturbance, essentially an overvoltage condition with increased levels of detected system voltages.

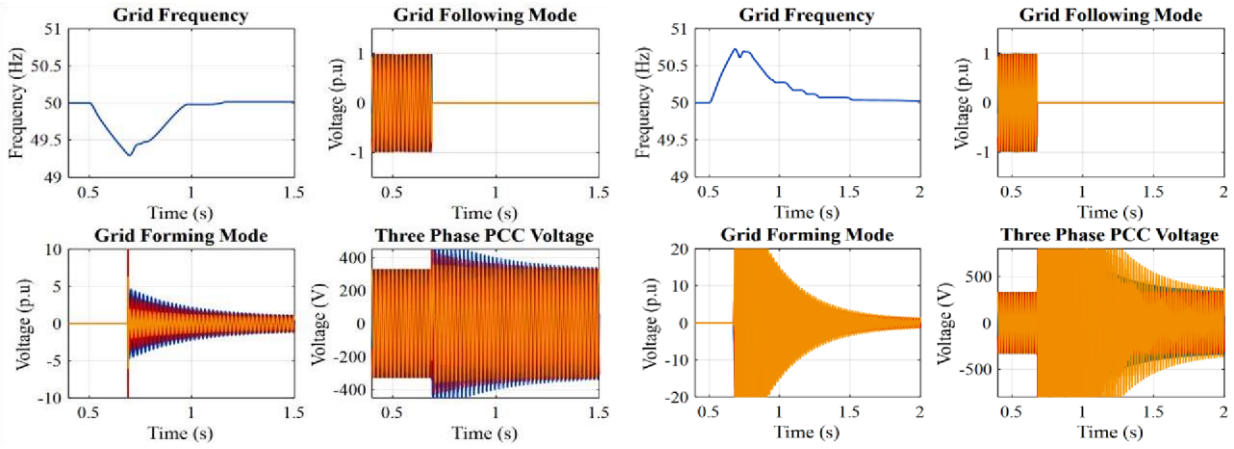

(a) **(b)**

Figure 14: Voltage and Frequency Profiles at Load End during (a) Under-Frequency Condition (b) Over-Frequency Condition

Thereafter, three-phase voltage and current stabilize at 0.705s or around 198.558ms following the initial overvoltage condition addressing. Following this transition, the converter switches to grid-forming mode, observed in the bottom graph. Once steady-state functioning is reached, no distortion or phase shift is seen, and the voltage waveform returns to its nominal amplitude while the current is balanced throughout all three phases. The active and reactive power at the load end during the transition from grid-following to grid-forming operation is shown in Figure 13(a). Initially, in the grid-connected mode, the converter supplies approximately 3.8kW of active power and 0.9kVAR of reactive

power. When under-voltage occurs at 0.517s, the power output drops significantly due to the grid disturbance. The converter subsequently switches from grid-following to grid-forming mode at 0.696s. Thus, allow it to re-establish power delivery. The waveforms show that both active and reactive power are fully stabilized within 215.611ms. The active and reactive power supplied at the load end is depicted in Figure 13(b). Initially, the power is supplied by the grid following a converter in the grid-connected mode. When the overvoltage occurred, the mode of the converter changed from grid-following mode to grid-forming mode at 0.692s. The output graphs of active and reactive power show that the power is stabilized within 210.598ms. The voltage profiles and system frequency at the load end demonstrate the system's dynamic response during the underfrequency event, as shown in Figure 14(a). In accordance with IEEE 1574 standards, an islanding condition is detected when the system frequency drops below 49.5Hz. This occurs when the frequency decreases to 49.5Hz at 0.938s of simulation, with islanding detection confirmed at 0.995s. The VSC mode of operation transitions from grid-following to grid-forming at 0.996s, executed within 57.323ms following the under-frequency event. The first plot illustrates the grid frequency declining from 50Hz to a minimum of 49.5Hz, the second plot shows the voltage in grid-following mode stabilizing at approximately 1p.u., the third plot indicates the voltage in grid-forming, and the fourth plot displays the three-phase PCC voltages.

For the over frequency condition, islanding begins when the system frequency rises above 50.5Hz at 0.909s. The islanding condition is detected at 0.971s. The VSC shifts from grid-following to grid-forming mode at 0.972s. The transition occurs 62.243ms after the frequency deviation. In grid-forming mode, the converter maintains voltage and frequency stability at the PCC. Figure 14(b) shows the system frequency, converter responses in both modes, and the voltage profiles at the PCC.

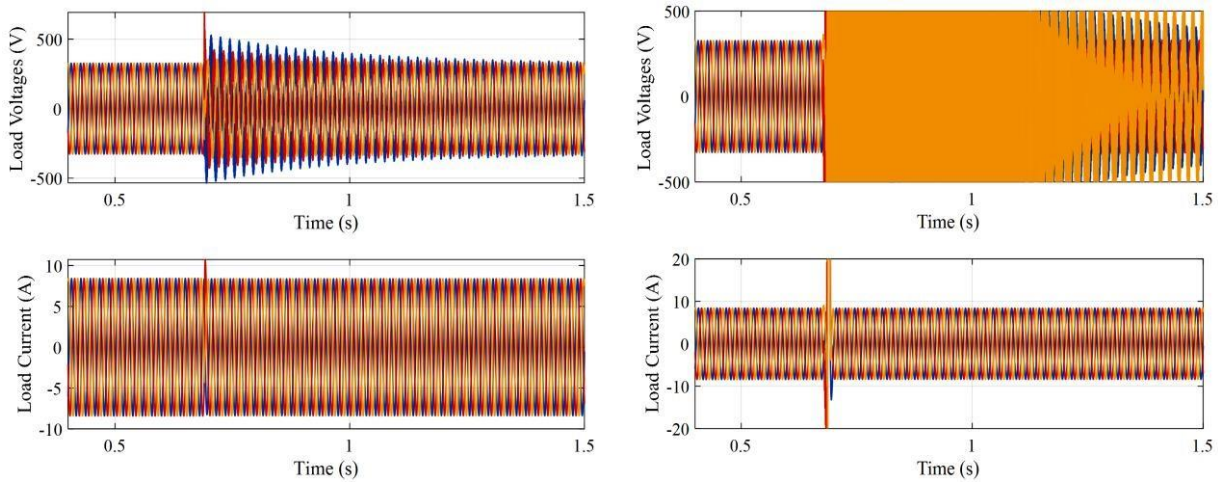

(a) **(b)**

Figure 15: Voltage and Current Profiles at Load End during (a) Under-Frequency Condition (a) Over-Frequency Condition

The three-phase output at the load end stabilizes at 1.005s after 67.057ms when under under-frequency condition is detected. The load remains supplied without interruption through the grid-forming mode of the converter. The voltage waveform shows a transient oscillation between 500V and 500V around 0.5s. It returns to steady state shortly after. The current waveform follows a similar pattern with amplitudes between 10A and 10A. Both voltage and current stabilize once the disturbance is cleared. Figure 15(a) shows the voltage and current waveforms at the load end during the underfrequency condition.

The three-phase output at the load end stabilizes at 0.986s. This occurs 77ms after the over-frequency condition is detected. The voltage waveform quickly returns to its nominal value, and the current remains balanced across all phases. Figure 15(b) shows the voltage and current waveforms at the load end during the over-frequency condition. When the grid is disconnected from the LV system due to a fault or disturbance, an islanding condition is detected.

The detection relay senses the event and switches the converter's mode of operation. In the simulation, the grid is disconnected at 0.5s. The voltage relay detects the voltage drop at the PCC and changes the VSC operation from grid-following to grid-forming mode at 0.692s. Figure 16 shows the grid voltages, PCC voltages, and the tripping command. The three-phase voltage at the PCC stabilizes within 307.851ms after grid disconnection. The active and reactive power profiles at the load end during grid disconnection are shown in Figure 17.

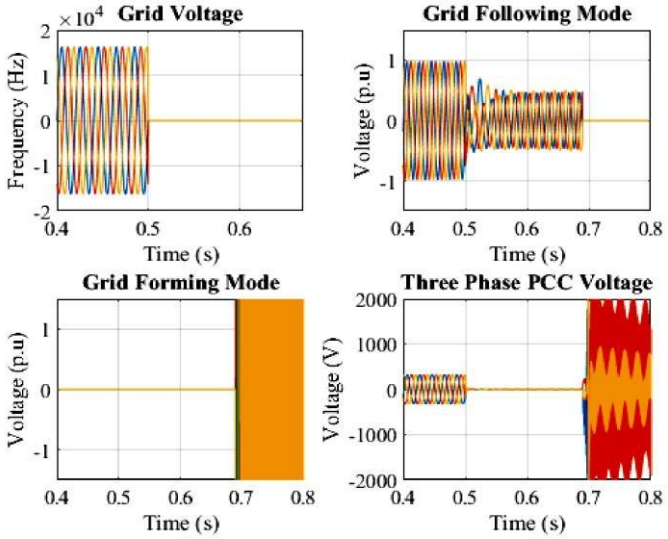

Figure 16: System response During Grid Disconnection

The active power exhibits a sharp dip, decreasing from approximately 4000W to 0W between 0.5s and 0.7s. This period represents the transition state, during which the load is temporarily unpowered. The reactive power also drops from around 1000VAR to 0VAR over the same interval. After 0.7s, both active and reactive power return to their nominal values of approximately 4000W and 1000VAR, respectively.

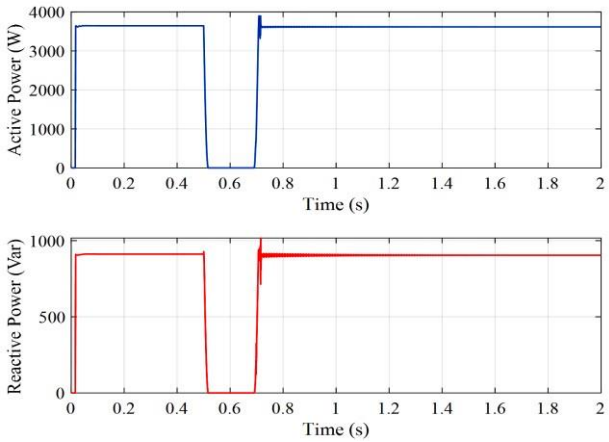

Figure 17: Active and Reactive Power Profiles at Load End During Grid Disconnection

The three-phase output at the load end remains unstable between 0.5s and 0.7s during the grid disconnection period, as shown in Figure 18. The voltage and current waveforms show discernible oscillations during this period. After 0.7s, the converter stabilizes and switches from grid following to grid-forming mode. The current stabilizes at 10A, and the RMS voltage reaches about 230V per phase. The system must recover within 200ms of disconnecting.

These control techniques under test are for islanding detection and VSC control, meant to improve response time as well as accuracy. An average value model, which makes computation easy, is used to portray the dynamic behavior

of the VSC. With this technique, the converter will be able to respond at full speed to any sudden changes in voltage or frequency emanating from grid interruptions.

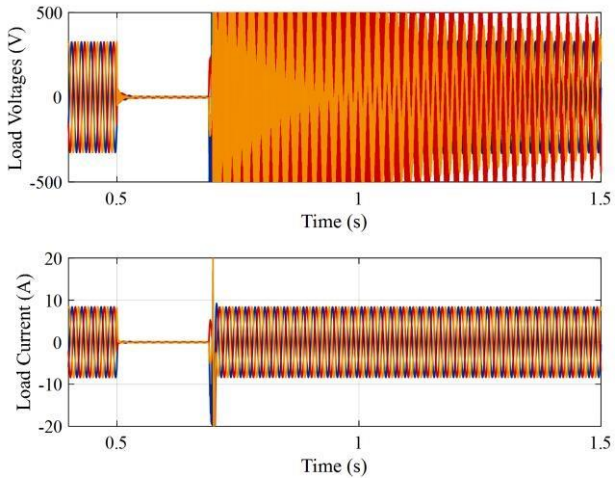

Figure 18: Voltages and Currents at Load End During Grid Disconnection

The simulation results of the proposed method under different operating conditions are listed in Table 3. It comprises under- and over-voltage, under- and over-frequency, and grid disconnect.

Table 3: Islanding Scenarios and Detection Time

Test Case	Scenario	Detection Time (ms)	UF	OF	UV	OV
1	Generator overloaded	67				
2	Generation in excess	77				
3	Load connection	189				
4	Load disconnection	198				
5	CB2 opens at the utility	204				

The results show that the control mechanism recognizes actual islanding occurrences with high accuracy and keeps the system stable with minimal disturbance.

Table 4: Comparison of Proposed and Conventional Methods

Test Case	Scenario	Proposed Method	Reference [20][21]
		Detection Time (ms)	Detection Time (ms)
1	Under Frequency	67	73
2	Over Frequency	77	79
3	Under Voltage	189	168
4	Over Voltage	198.6	151

A comparison between the proposed relay schemes and conventional methods is provided in Table 4. The proposed frequency relay was compared with the Rate of Change of Frequency (ROCOF) relay developed in [11], while the voltage relay was tested against the OUV relay from [14]. During the over-frequency event at 0.8s, the proposed relay

issued a trip signal in 0.92ms while the ROCOF relay took 1.18ms. The proposed relay responded to under-voltage (at 0.5s) in 90.74ms, whereas the OUV relay took 99.21ms. These findings verify that the improved relays detect faults more quickly and increase the stability and dependability of the VSC's mode transition under islanding conditions.

V. CONCLUSION

This paper introduces an islanding detection mechanism with a control methodology for switching the operational state of the voltage source converter from grid-following to grid-forming. Simulations are provided for over/undervoltage, over/under-frequency, and grid detection schemes using the average VSC model at low voltage. As a result, it correctly shows a distributed generator that is located at the customer's location. System performance is assessed using the CIGRE low-voltage test network. Analysis of the VSC islanding detection system reveals that the proposed scheme, designed for frequency-voltage variation detection, can attain better performance with reduced detection time as well as reduced power losses and disturbances in the converter output. Thus, sustaining the delivery of stable power to the load at PCC. After comparative evaluation with other detection relays, it has been proven that the proposed approach works well.

The proposed islanding detection system provides essential operational benefits through its quick and stable detection capabilities, which allow for automatic grid forming operation to start immediately. The system detects islanding quickly and performs automatic grid forming operations to provide safety benefits and reduce equipment stress and power quality disturbances, while maintaining critical load continuity in high DER low voltage networks. The system provides fast detection along with minimal power losses, which makes it suitable for microgrids and residential solar systems, and IEEE 1547 compliance. The research needs to continue with hardware-in-the-loop testing and field validation. It needs to connect with energy storage systems and machine learning prediction systems, and needs to apply to medium voltage systems, and establish standardized detection thresholds for smart distribution grid deployment.

REFERENCES

[1] J. A. Cebollero, D. Cañete, S. Martín-Arroyo, M. García-Gracia, and H. Leite, “A survey of islanding detection methods for microgrids and assessment of non-detection zones in comparison with grid codes,” Energies, vol. 15, no. 2, 2022, doi: 10.3390/en15020460.

[2] S. Sarangi, B. K. Sahu, and P. K. Rout, “An advanced fault detection technique for DG integrated microgrid using fast Fourier discrete orthonormal Stockwell transform-based hybrid optimized kernel extreme learning machine,” Iranian Journal of Science and Technology, Transactions of Electrical Engineering, vol. 46, no. 2, pp. 329–351, 2022, doi: 10.1007/s40998-022-00481-w.

[3] L. Ortiz, R. Orizondo, A. Águila, J. W. González, G. J. López, and I. Isaac, “Hybrid AC/DC microgrid test system simulation: Grid-connected mode,” Heliyon, vol. 5, no. 12, 2019, doi: 10.1016/j.heliyon.2019.e02862.

[4] P. Kumar, V. Kumar, and B. Tyagi, “Islanding detection for reconfigurable microgrid with RES,” IET Generation, Transmission & Distribution, vol. 15, no. 7, pp. 1187–1202, Apr. 2021.

[5] A. K. Nanda, B. Panda, and C. K. Panigrahi, “A review on control technologies and islanding issues in microgrids,” in Renewable Energy and Sustainable Growth Assessment, pp. 475–502, 2022, doi: 10.1002/9781119785460.ch17.

[6] V. Panchal, A. Swarnkar, N. Gupta, and K. R. Niazi, “Comparative study of islanding detection techniques of microgrid for solar PV as distribution generator,” Lecture Notes in Electrical Engineering, vol. 862, pp. 635–648, 2022, doi: 10.1007/978-981-19-0252-9_57.

[7] E. Song, A. F. Lynch, and V. Dinavahi, “Experimental validation of nonlinear control for a voltage source converter,” IEEE Transactions on Control Systems Technology, vol. 17, no. 5, pp. 1135–1144, Sep. 2009.

[8] M. P. Kazmierkowski, R. Krishnan, F. Blaabjerg, and J. D. Irwin, Control in Power Electronics: Selected Problems, 1st ed. New York, NY, USA: Academic Press, 2002.

[9] A. Ghaderi and M. Kalantar, “Investigation of influential factors on passive islanding detection methods of inverter-based distributed generation,” Proc. 2nd Power Electronics, Drive Systems and Technologies Conf. (PEDSTC), pp. 217–222, 2011, doi: 10.1109/PEDSTC.2011.5742421.

[10] A. Hoke and D. Maksimović, "Active power control of photovoltaic power systems," Proc. IEEE Conf. Technologies for Sustainability (SusTech), pp. 70–77, 2013, doi: 10.1109/SusTech.2013.6617300.

[11] I. V. Banu, M. Istrate, D. Machidon, and R. Pantelimon, "A study on anti-islanding detection algorithms for grid-tied photovoltaic systems," Proc. Int. Conf. Optimization of Electrical and Electronic Equipment (OPTIM), pp. 655–660, 2014, doi: 10.1109/OPTIM.2014.6850940.

[12] V. Mohan, R. Suresh, J. G. Singh, W. Ongsakul, and N. Madhu, "Microgrid energy management combining sensitivities, interval and probabilistic uncertainties of renewable generation and loads," IEEE J. Emerg. Sel. Top. Circuits Syst., vol. 7, no. 2, pp. 262–270, 2017, doi: 10.1109/JETCAS.2017.2679030.

[13] A. Aghazadeh, M. Davari, H. Nafisi, and F. Blaabjerg, "Grid integration of a dual two-level voltage-source inverter considering grid impedance and phase-locked loop," IEEE J. Emerg. Sel. Top. Power Electron., vol. 9, no. 1, pp. 401–422, 2021, doi: 10.1109/JESTPE.2019.2953522.

[14] K. R. Waghare and N. R. Bhasme, "Islanding detection of distributed generation in the presence of fault events with critical and non-critical loads," Int. J. Eng. Adv. Technol., vol. 9, no. 1, pp. 3293–3297, 2019.

[15] S. Sayed and A. Massoud, "A MATLAB/Simulink-based average-value model of multi-terminal HVDC network," Proc. Int. Conf. Smart Grid Renew. Energy, pp. 1–6, 2019.

[16] Y. A. Elshrief et al., "Fast and accurate islanding detection technique for microgrid connected to photovoltaic system," J. Radiat. Res. Appl. Sci., vol. 14, no. 1, pp. 210–221, 2021.

[17] S. Hasan and S. S. Saleh, "A new passive islanding detection technique for a microgrid based on transient energy," IET Gener. Transm. Distrib., vol. 16, no. 12, pp. 2476–2500, 2022.

[18] M. Chen et al., "Generalized multivariable grid-forming control design for power converters," IEEE Trans. Smart Grid, vol. 13, no. 4, pp. 2873–2885, 2022.

[19] Y. Luo, I. U. Nutkani, and L. Meegahapola, "Adaptive protection scheme with passive islanding detection for AC microgrids," Proc. IEEE IPEC-Himeji, pp. 1584–1591, 2022.

[20] Y. Zhou et al., "Small-signal stability assessment of heterogeneous grid-following converter power systems based on grid strength analysis," IEEE Trans. Power Syst., vol. 38, no. 3, pp. 2566–2579, 2023.

[21] H. Zheng et al., "An islanding detection method using synchronized small-AC-signal injection for grid-forming inverters in microgrids," IEEE Trans. Power Electron., vol. 38, no. 5, pp. 5816–5831, 2023.

[22] C. R. Ramos et al., "Impacts of output voltage control on PV generation islanding detection function," Electr. Power Syst. Res., vol. 235, p. 110897, 2024.

[23] S. T. Chauhdary et al., "Fast passive anti-islanding strategy for AC microgrids using cubature Kalman filtering algorithm," IEEE Access, vol. 12, pp. 85608–85621, 2024.

[24] Schneider Electric, "Minera-ground transformer product datasheet," Dec. 2022. [Online]. Available: https://www.se.com